Thermal analysis of high-performance mid-infrared quantum cascade lasers

H. K. Lee and J. S. Yu*
Department of Electronic and Radio Engineering, Kyung Hee University, Yongin 446-701, Korea
*jsyu@khu.ac.kr

***Abstract*-We investigated theoretically the thermal characteristics of quantum cascade lasers (QCLs) based on InGaAs/AlInAs/InP materials operating at λ~ 4.6 μm. By using a steady-state two dimensional (2D) heat dissipation model, the maximum internal temperature, heat flow pattern, and thermal conductance were obtained for the different device geometries with epilayer-up and down bonding scheme. As the heatsink temperature increases, the maximum internal temperature increases. For 10 μm x 4 mm epilayer-down bonded laser with diamond submount and InP waveguide, a high thermal conductance of G_{th}= 619.7 W/K-cm^2 at room temperature was obtained.**

I. INTRODUCTION

The high-performance mid-wavelength infrared (MWIR) quantum cascade lasers (QCLs) are very important as the most promising light source for various applications [1]. In particular, the applications such as remote systems and pollution monitoring need high power continuous-wave (CW) QCLs above room temperature. However, the QCL is an inherently high heating device due to the high electrical power density for lasing. This makes it difficult to obtain high power and CW operation at room temperature.

Recently, MWIR QCLs emitting a watt-level CW output power were reported using improved device designs, process techniques, and thermal packaging [2, 3]. Although the very high output power CW operation above room temperature has been demonstrated experimentally, there is little theoretical thermal analysis of MWIR QCL structures in details. In order to have a deep insight into the thermal behavior for QCL structures, the thermal modeling using a finite element method (FEM) is crucial. The thermal analysis makes it possible to optimize the device structures for more efficient heat dissipation.

In this presentation, we investigate the thermal characteristics of the double-channel ridge waveguide QCL by the two dimensional (2D) FEM model using the COMSOL. Also, the simulation focused on the thermal analysis of QCL structures to improve the thermal properties from the reported experimental data.

II. THERMAL MODEL AND PARAMETER

For the thermal analysis, we investigated the actual device structures reported in Refs. [2] and [3]. The devices with double-channel (DC) ridge waveguide are based on InGaAs/AlInAs/InP materials. The QCLs consisted of 30 active/injector stages (i.e. ~ 1.47 μm in Ref. [2] and ~ 1.4 μm in Ref. [3]) indicated a thickness of ~ 10 μm wide ridge width. The ridge width is defined by the average width of active core. The devices were bonded epilayer-up onto a copper heatsink. For an epilayer-down bonding, the devices were bonded onto AlN and diamond submounts, and then they were bonded onto the copper heatsink with indium solder.

In order to obtain temperature profile, heat flow, and thermal conductance of QCL structures, the thermal simulation was carried out by a steady-state 2D anisotropic heat dissipation model. The generated heat from the active core region is transferred from the internal region of the device to the atmosphere by convection. But a large proportion of generated heat is transferred through the InP substrate, submount to the copper heatsink by conduction. The steady-state 2D anisotropic heat transfer equation is given by [4]

$$Q = -\nabla \cdot (k \nabla T), \quad (1)$$

$$k \nabla T = h(T_{\inf} - T), \quad (2)$$

where T is the temperature, Q is the power density dissipated in active core region, h is the heat transfer coefficient (h = 20 W/m^2-K for natural convection), and T_{inf} is the ambient temperature. We used temperature-dependent thermal conductivities for more reasonable thermal analysis. Also, all the layers except for the active core region were considered as isotropic materials. For the activity core layer, we take into account an anisotropic thermal conductivity ($k_{\parallel} \neq k_{\perp}$) due to interface effects [5]. The in-plane $k_{\parallel}$ value was estimated as 75% of the weighted average value of the active core region constituent materials. The cross-plane $k_{\perp}$ value was extracted from experimental data as only fitting parameter. The thermal conductivities as a function of temperature used in this simulation are listed in Table I [6-7].

TABLE I
TEMPERATURE-DEPENDENCE THERMAL CONDUCTIVITIES

Materials	Thermal conductivity (W/m-K)
InP	$2.82 \times 10^{5} T^{-1.45}$
GaInAs	$23-9.3 \times 10^{-2} T+1.06 \times 10^{-4} T^{2}$
SiO_2	$974 \times 10^{-4}+538 \times 10^{-5} T-469 \times 10^{-8} T^{2}$
Au	$337-660 \times 10^{-4} T$
In	$93.9-696 \times 10^{-4} T+986 \times 10^{-7} T^{2}$
Ti	$31.46-4338 \times 10^{-5} T+4 \times 10^{-5} T^{2}$
Cu	$349+14710 T^{-1}$

978-1-4244-4180-8/09/$25.00 ©2009 IEEE

AlN	$1540\text{-}6T+5.75\times10^{-3}T^2$
Diamond	$4.35\times10^{6}T^{-1.3}$
Active core region	$k_{\parallel}= 5.3\text{-}3.9\times10^{-3}T+5.3\times10^{-7}T^2$, $k_{\perp}= 2.4\pm1$

III. RESULTS AND DISCUSSION

Fig. 1 shows the maximum internal temperature of DC QCLs as a function of heatsink temperature for different geometries and bonding schemes. The inset shows the maximum internal temperature of active core region as a function of injection current. As shown in Fig. 1, the maximum internal temperature increases with increasing heatsink temperature. Because the increased heatsink temperature leads to higher threshold current, the internal temperature increases. In the case of Ref. [2] with epilayer-up bonding scheme, the maximum internal temperature at room temperature indicated a value of 397 K for L= 1.5 mm. it was increased by 44 K compared to a value of 353 K for L= 4 mm. The heat source of devices increases for shorter cavity due to the increased mirror loss. That is, the long cavity length allows the device to operate with higher maximum CW operating temperature. For the structure of Ref. [3], the use of InP waveguide and diamond submount with high thermal conductivity improve significantly the heat extraction capability. Furthermore, 4 μm thick electroplated Au around the laser ridge leads to the better lateral heat removal from the active core. Thus, the maximum internal temperature at room temperature was improved by 23.3 K compared to that of the epilayer-down bonded layer with InGaAs waveguide and AlN submount.

Fig. 2 shows the thermal conductance as a function of heatsink temperature for various device geometries with L= 4 mm. As shown in figure 2, the use of InP waveguide and epilayer-down bonding scheme shows the improved thermal conductance. It is clear that the thermal conductance is improved using all these combinations such as InP waveguide, buried heterostructure, and diamond submount. However, the use of AlN submount decrease the thermal conductance compared to that of the device structure without submount. In the case of the DC ridge structure with diamond submount and InP waveguide, it exhibited slightly lower G_{th} (i.e. by 8 W/K-cm^2, indicating a temperature difference of 0.2 K) compared to the structure with all combinations. That is, the use of diamond submount can improve the thermal properties with a simple process. For epilayer-down bonding with diamond submount and InP waveguide, the thermal conductance indicated a high G_{th}= 619.7 W/K-cm^2 at room temperature.

IV. CONCLUSIONS

We analyzed the theoretically temperature distribution, maximum internal temperature, and thermal conductance of DC ridge QCL lasers with various geometries and bonding schemes. As the heatsink temperature increases, the maximum internal temperature increases. The long cavity length allows for a higher maximum CW operating temperature. As a result, for epilayer-down bonding with diamond submount and InP waveguide, the thermal conductance of a high G_{th}= 619.7 W/K-cm^2 at room temperature was obtained.

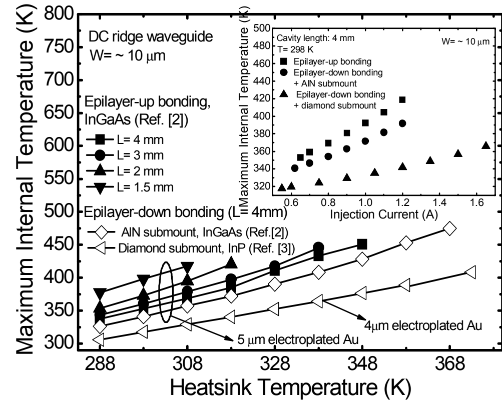

Fig. 1. Maximum internal temperature as a function of heatsink temperature with different geometries and bonding schemes.

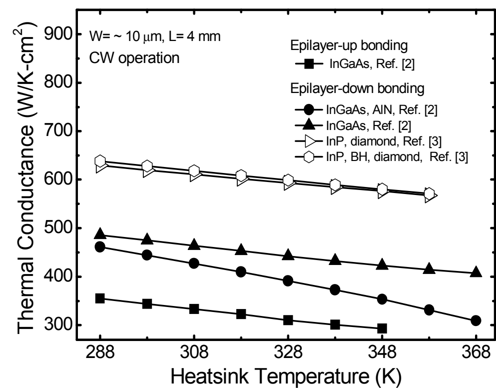

Fig. 2. Thermal conductance as a function of heatsink temperature with different geometries and bonding schemes.

REFERENCES

[1] F. Capasso, C. Gmachl. Gmachl, R. Paiella, A. Tredicucci, A.L. Hutchinson, D.L. Sivco, J.N. Baillargeon, A.Y. Cho, H.C. Liu, IEEE J. Sel. Top. Quamtum Electron. **6**, 931 (2000).

[2] J.S. Yu, S. Slivken, A. Evans, M. Razeghi, IEEE J. Quamtum Electron. **44**, 747 (2008).

[3] Y. Bai, S. Slivken, S. R. Darvish, M. Razeghi, Appl. Phys. Lett. **93**, 021103 (2008).

[4] C. zhu, Y. Zhang, A. Lie, and Z. Tian, J. Appl. Phys. 100, 053105 (2006)

[5] A. Lops, V. Spagnolo, and G. Scamarcio, J. Appl. Phys. **100**, 043109 (2006).

[6] C. A. Evans, D. Indjin, Z. Ikonic, P. Harrison, IEEE J. Quantum Electron. **44**, 680 (2008).

[7] V. Spagnolo, A. Lops, G. Scamarcio, M. S. Vitiello, and C. D. Franco, J. Appl. Phys. **103**, 043103 (2008).